# Modification of $n = 0$ Equatorial Waves Due to Interaction between Convection and Dynamics

PRASHANTH GOSWAMI AND B. N. GOSWAMI

*Centre for Atmospheric Sciences, Indian Institute of Science, Bangalore, India*

(Manuscript received 22 June 1990, in final form 1 April 1991)

ABSTRACT

A mechanism is proposed that can sustain unstable equatorially trapped westward-propagating low-frequency modes in the tropics. The roles of evaporation–wind feedback and wave–CISK (convergence feedback) in modifying the $n = 0$ equatorially trapped modes are studied. It is shown that the convergence feedback by itself cannot make the waves unstable but can modulate the instability introduced by evaporation–wind feedback. We show that the evaporation–wind feedback introduces a new westward-propagating $n = 0$ mode in addition to dramatically modifying the dry mixed Rossby–gravity (MRG) mode. The new mode is generally damped for mean background easterlies but can be nearly neutral for moderate strength of evaporation–wind feedback and strong convergence feedback. The evaporation–wind feedback makes the MRG mode unstable in a westward-propagating low-frequency regime and in an eastward-propagating high-frequency regime. If the background mean winds are easterlies, the gravest low-frequency mode resembles the westward-propagating mode with period of about 4 days and wavelength of about 7000 km observed over the central and western Pacific. The evaporation–wind feedback also makes the meridional structure of the eigenfunctions of these modes frequency dependent. The low-frequency waves are more tightly trapped around the equator as compared to their high-frequency counterparts. It also introduces a meridional propagation for the mode. The sensitivity of the characteristics of the gravest low-frequency mode to variations of the strength of the two feedbacks is discussed.

## 1. Introduction

In recent years, the modifications of the equatorial Kelvin wave by moist processes have been studied extensively to explain the eastward-propagating 30–60-day oscillations in the tropics (Madden and Julian 1971, 1972; Knutson and Weickman 1987; Murakami and Nakazawa 1985; Madden 1986; Lau and Chan 1986; Krishnamurti et al. 1985; Weickman et al. 1985). It was Parker (1973) who first suggested that this eastward-propagating intraseasonal oscillation may be related to the equatorial Kelvin mode. However, a dry Kelvin wave in an inviscid atmosphere cannot explain the observed period, as its period with observed spectral structure would be only about ten days. Following observational evidence that this oscillation is associated with deep convection, many recent studies (Takahashi 1987; Lau and Peng 1987; Yamagata 1987; Hendon 1988; Miyahara 1987; etc.) have involved Kelvin wave with various forms of wave–CISK. In general, introduction of wave–CISK feedback slows the eastward propagation of the Kelvin wave. Another mechanism, known as evaporation–wind feedback, is based on the recognition that mean winds in the equatorial region are mostly easterly. In the presence of mean background easterlies, the Kelvin response to the east of an equatorial heat source enhances the evaporation on the eastern side of the heat source, while the Rossby response to the west reduces evaporation on the western side of a heat source. This process makes the heat source slowly move eastward. Emanuel (1987), Neelin et al. (1987), and Lau and Shen (1988) have shown that with mean easterlies, eastward-propagating Kelvin waves with intraseasonal period may be unstable when the moist static stability is everywhere neutral.

The studies just cited were all aimed at explaining the eastward-propagating equatorial 30–60-day oscillations. As a result, all these analytical studies examined the modification of the equatorial Kelvin wave by wave–CISK and evaporation–wind feedback. To our knowledge, no one thus far has examined how the mixed Rossby–gravity (MRG) wave is modified by these feedback processes. However, the MRG wave plays an equally important role in tropical dynamics. Therefore, in this study we have concentrated only on the modification of the MRG wave by wave–CISK and evaporation–wind feedback. We are further motivated by recent observations of westward-propagating waves in the tropics whose sources have not been adequately explained. For example, Takayabu and Murakami (1991) report observations of westward-propagating waves, with period of 3–4 days and wavelengths of the order of 6000 km, embedded within eastward-propagating super cloud clusters (SCC) in the western Pacific.

*Corresponding author address:* B. Goswami, Centre for Atmospheric Sciences, Indian Institute of Science, Bangalore 560 012 India.

They also examined objectively analyzed global winds and geopotential height fields for the period concurrent with the SCC observations. Associated with the westward-propagating waves in the SCC, the analyzed fields show oscillations mainly in the lower troposphere. Moreover, the fluctuations in the same frequency range on the meridional velocity show maximum amplitude over the equator, while those on the zonal wind show maximum amplitude around 7.5°N and 7.5°S. This indicates that these waves may be MRG waves. However, the source of energy for these waves remained unclear. In another recent study, Liebmann and Hendon (1990) examined spectrally eight years (1980–87) of initialized wind analysis at the European Centre for Medium Range Weather Forecasting and OLR data. They found significant power in the frequency range with periods between 3.5 days and 6 days over the western Pacific and Atlantic. These are westward-propagating waves with wavelengths between 6000 and 7000 km. They also show that the maximum amplitude of these westward-propagating synoptic waves is in the lower troposphere. Their analysis also indicates that these may be equatorially trapped MRG waves. In this study we indicate a source for these observed westward-propagating MRG waves and show that the evaporation–wind feedback can drive the MRG wave unstable and that the convergence feedback (wave–CISK) influences the magnitude of this instability. For reasonable strengths of the convergence feedback and the evaporation–wind feedback, the growth rate has a maximum with a period between 3 and 6 days, having a wavelength around 8000 km.

## 2. Model equations and method of solution

We use the shallow-water equations describing the horizontal structure of the first baroclinic mode in this study. The basic equations, used in many studies of intraseasonal oscillations in the tropics (Davey 1985; Lau and Shen 1988; Davey and Gill 1989), may be written as

$$\frac{\partial u}{\partial t} - fv = \frac{C_0^2}{\theta_0}\frac{\partial \theta}{\partial x} - Ru, \tag{1}$$

$$\frac{\partial v}{\partial t} + fu = \frac{C_0^2}{\theta_0}\frac{\partial \theta}{\partial y} - Rv, \tag{2}$$

$$\frac{\partial \theta}{\partial t} - H\frac{d\theta_0}{dz}\left(\frac{\partial u}{\partial x} + \frac{\partial v}{\partial y}\right) = Q - R\theta, \tag{3}$$

$$\frac{\partial q}{\partial t} + q_s\left(\frac{\partial u}{\partial x} + \frac{\partial v}{\partial y}\right) = E - P, \tag{4}$$

where $u$, $v$ are the zonal and meridional perturbation velocities in the lower layer, $\theta$ the midlevel perturbation potential temperature with $\pi H$ and $\theta_0$ representing tropopause height and midlevel mean potential temperature. $Q$ represents perturbation heating while $R$ represents a Raleigh friction coefficient. Although, in general, the Raleigh friction and the thermal damping coefficient (or Newtonian cooling coefficient) may be different, we shall restrict ourselves to the case when they are equal. For the major part of our discussion, we shall consider the frictionless case ($R = 0$) and later show how small friction would modify these results. Equation (4) describes the evolution of the perturbation moisture content $q$ in units of mass of precipitable water per unit area with $q_s$ representing the saturated moisture content. In Eq. (4) $E$ and $P$ represent perturbation surface evaporation and precipitation, respectively, both in units of mass per unit area per unit time.

The physics of our system is contained in the terms $Q$, $E$, and $P$. First we discuss parameterization of the heating rate $Q$. Here we follow arguments given by Gill (1982), Davey (1985, 1989), and Lau and Shen (1988). In general, we can conceive two different regimes in the tropical atmosphere, a "convective" regime where the atmosphere remains saturated and a "nonconvective" regime where part of the converged moisture goes into moistening the atmosphere. For simplicity we assume that the tropical atmosphere is always near saturation and hence always in the convective regime. In this case, the moisture gained by convergence and evaporation is depleted by precipitation, and we can write

$$q_s\left(\frac{\partial u}{\partial x} + \frac{\partial v}{\partial y}\right) = E - P. \tag{5}$$

If we assume that the latent heat released during precipitation is distributed uniformly over the lower atmosphere of depth $H$, the heating rate, $Q$, may be written as

$$Q = \frac{LP}{\rho_a c_p H} \tag{6}$$

where $\rho_a$ is the density of air, $L$ the latent heat of condensation, and $c_p$ the specific heat at constant pressure.

Our next step involves parameterization of perturbation evaporation. Following arguments similar to ones given by Neelin et al. (1987), we can write

$$E = -\alpha u, \tag{7}$$

with $\alpha = \rho_a C_D \Delta q_s$, where $C_D$ is the drag coefficient and $\Delta q_s$ represents the saturation relative humidity difference between the sea surface and the anemometer level. In Eq. (7) $\alpha$ depends on the sign of the mean zonal wind $\bar{u}$ and has been chosen in such a way that $\alpha$ is positive for mean easterlies and negative for mean westerlies. Since $\bar{u}$ is mostly easterly over the tropics, $\alpha$ will be considered positive in our study. Thus, substituting Eqs. (5)–(7), Eq. (3) may be written entirely in terms of $\theta$, $u$, and $v$, closing the set of equations (1)–(3). We define the following length scale $L_0$, time

scale $T_0$, velocity scale $C_0$, and a scale for the potential temperature perturbation $\Theta$:

$$\left.\begin{aligned} C_0 &= \{(d\theta_0/dz)/g\theta_0\}^{1/2}H \\ L_0 &= (C_0/2\beta_0)^{1/2} \\ T_0 &= (2C_0\beta_0)^{-1/2} \\ \Theta &= Hd\theta_0/dz \end{aligned}\right\}. \quad (8)$$

Here $\beta_0$ is the north–south gradient of the Coriolis parameter at the equator.

Equations (1)–(3) can be written in nondimensional form as

$$\frac{\partial u}{\partial t} - fv + Ru = \frac{\partial \theta}{\partial x}, \quad (9a)$$

$$\frac{\partial v}{\partial t} + fu + Ru = \frac{\partial \theta}{\partial y}, \quad (9b)$$

$$\frac{\partial \theta}{\partial t} - \Gamma\left(\frac{\partial u}{\partial x} + \frac{\partial v}{\partial y}\right) + \Lambda u + R\theta = 0, \quad (9c)$$

where

$$\Gamma = 1 - \frac{q_s}{q_{\text{crit}}}, \quad \Lambda = \alpha^* \frac{L_0}{q_{\text{crit}}},$$

$$\alpha^* = \frac{\alpha}{\rho_w}, \quad q_{\text{crit}} = \rho_a c_p H^2 \frac{(d\theta_0/dz)}{L\rho_w}. \quad (10)$$

In Eq. (9), $R = R^*T_0$, $f = \beta y$ with $\beta = \frac{1}{2}$, and * represents the dimensional quantities. We note that $q_{\text{crit}}$ represents a critical value of liquid water content (expressed in units of length) and $\Gamma$ the reduced static stability parameter. Here $\Gamma = 1$ represents the case without convergence feedback, and $\Gamma = 0$ the moist-neutral case. The standard parameters used for the model atmosphere are (e.g., see Davey and Budin 1989) $\theta_0 = 310$ K, $d\theta_0/dz = 3.89 \times 10^{-3}$ K m$^{-1}$, $H = 17\,000/\pi$ m, $\rho_a = 1.225$ kg m$^{-3}$, $\rho_w = 10^3$ kg m$^{-3}$, and $C_D = 1.5 \times 10^{-3}$. With these parameters, the speed of the dry gravity waves, $C_0$, is approximately 60 m s$^{-1}$. With $\beta_0 = 2.28 \times 10^{-11}$ m$^{-1}$ s$^{-1}$, our length scale, $L_0$, is approximately 10 deg and our time scale, $T_0$, is approximately 0.22 days. Using these parameters, $q_{\text{crit}}$ in our model is found to be about 6 cm and the scale for potential temperature perturbation is about 30 K. Assuming a variation of $\Delta q_s$ between 0% and 10%, a variation of the nondimensional strength of evaporation wind feedback ($\Lambda$) between 0 and 2 is considered.

Let us assume a solution in the form of wave propagating in the east–west direction, so that we may write

$$\xi(x, y, t) = \xi(y) \exp\{i(kx - \omega t)\}, \quad (11)$$

where $\xi$ represents any of the variables $u$, $v$, or $\theta$; $k$ is the wavenumber in the zonal direction and $\omega$ the frequency. Substituting Eq. (11) in Eqs. (9), we get

$$\sigma u - ifv + k\theta = 0, \quad (12.1)$$

$$\sigma v + ifu - i\frac{d\theta}{dy} = 0, \quad (12.2)$$

$$\sigma\theta + \hat{\Gamma}u - i\Gamma\frac{dv}{dy} = 0, \quad (12.3)$$

where

$$\sigma = \omega + iR, \quad \hat{\Gamma} = \Gamma k + i\Lambda. \quad (12.4)$$

In Eq. (12), $u$, $v$, and $\theta$ now represent only the $y$-dependent parts. Eliminating $u$ and $\theta$ from the Eqs. (12.1)–(12.3), we can derive an equation for $v$, which may be written as

$$\frac{d^2v}{dy^2} + M(y)\frac{dv}{dy} + N(y)v = 0, \quad (13)$$

where

$$M(y) = -\frac{i\Lambda f}{\sigma\Gamma}, \quad (14.1)$$

and

$$N(y) = \Gamma^{-1}\left\{\sigma^2 - f^2 - \hat{\Gamma}k - \hat{\Gamma}\sigma^{-1}\frac{df}{dy}\right\}. \quad (14.2)$$

First, making a dependent variable transformation given by

$$v(y) = V(y)\exp\left\{-\frac{1}{2}\int M(y)dy\right\} \quad (14.3)$$

and then making an independent variable transformation given by $\Psi = C_1^{1/4}y$, Eq. (13) may be rewritten as

$$\frac{d^2V}{d\Psi^2} + (C_2C_1^{-1/2} - \Psi^2)V = 0, \quad (15)$$

where

$$C_1 = \beta^2\Gamma^{-1}\{1 + \Lambda^2/(4\sigma^2\Gamma)\} \quad (16.1)$$

and

$$C_2 = \Gamma^{-1}\{\sigma^2 - \Gamma k^2 - i\Lambda k\} - \beta\sigma^{-1}\Gamma^{-1}(\Gamma k + i\Lambda/2). \quad (16.2)$$

Since we shall be restricting ourselves to the equatorial waves only, we demand boundary conditions such that $V = 0$ as $\Psi \to \pm\infty$. With these boundary conditions, Eq. (15) has solutions in the form

$$V(\Psi) = Ce^{-\Psi^2/2}H_n(\Psi), \quad (17)$$

where $H_n(\Psi)$ represents Hermite polynomial of order $n$.

These equatorially trapped ($v = 0$, as $y \to \pm\infty$) plane waves, governed by Eq. (9), follow an energy integral constraint. Defining an energy of the wave perturbation by $E = (u^2 + v^2 + \theta^2/\Gamma)/2$ and making use of periodic condition in the zonal direction, an energy integral equation can be derived from Eq. (9). For the nondissipative case ($R = 0$), this equation may be written as

$$\frac{\partial}{\partial t}\langle E\rangle = -\frac{\Lambda}{\Gamma}\langle u\theta\rangle,$$

where $\langle\ \rangle$ represents an integral over one wavelength in the $x$ direction and between $\pm\infty$ in the $y$ direction. It is clear from this equation that in the absence of evaporation–wind feedback ($\Lambda = 0$), there is no source of energy for the waves to grow. However, in the presence of evaporation–wind feedback and if phases of $u$ and $\theta$ are shifted in such a way that $\langle u\theta\rangle$ is negative, the wave can grow exponentially in time. Physically, this can be understood as follows. If the region of positive potential temperature perturbation coincides with easterly wind perturbations, the wind perturbations enhance evaporation, hence enhancing the convective heating over that region. This further increases a positive $\theta$ perturbation leading to growth of the wave as a whole.

## 3. The dispersion relation

The solution given by Eq. (17) is possible only when

$$C_2C_1^{-1/2} = 2n + 1, \quad n = 0, 1, 2, \cdots. \tag{18}$$

With $C_1$ and $C_2$ as defined in Eq. (16), Eq. (18) represents the dispersion relation for the equatorial waves modified by the feedback processes.

In the absence of the feedback processes, Eq. (18) contains for $n \geq 1$ the westward-propagating low-frequency Rossby waves and pairs of eastward- and westward-propagating high-frequency inertia gravity (IG) waves. For $n = 0$, it contains the westward-propagating Rossby–gravity wave that merges with an eastward-propagating IG wave at wavenumber $k = 0$. It also contains a westward-propagating Kelvin-like wave whose eigenfunctions are unbounded and, hence, is not allowed. Apart from these normal modes, Eq. (12) also allows an eastward-propagating Kelvin mode with $v = 0$. Several authors (Neelin et al. 1987; Emanuel 1987; Lau and Shen 1988) studied the effect of the feedbacks on the Kelvin mode. Thus, we shall not repeat these results. The other mode that plays an important role in the tropical dynamics is the $n = 0$ mixed Rossby–gravity mode. Therefore, in this study we shall examine in detail the modification of the $n = 0$ modes by the feedback processes described earlier. In studying the dispersion relation we shall follow the convention where we assume the frequency $\omega$ to be positive definite and solve for the wavenumber $k$, which may be complex (Pedlosky 1979).

Using the definitions of $C_1$ and $C_2$ given in Eq. (16), for $n = 0$, Eq. (18) may be reduced to a pair of quadratic equations (one with $A^+$, the other with $A^-$) in wavenumber $k$ given by

$$k^2 + \left\{\frac{\omega\beta}{\omega^2 + R^2} + i\left(\frac{\Lambda}{\Gamma} - \frac{R\beta}{\omega^2 + R^2}\right)\right\}k + A^{\pm} + A_0 = 0, \tag{19}$$

where

$$A_0 = -\frac{1}{\Gamma}\left[\omega^2 - R\left\{R + \frac{\Lambda\beta}{2(\omega^2 + R^2)}\right\} + i\left\{2\omega R - \frac{\Lambda\beta\omega}{2(\omega^2 + R^2)}\right\}\right], \tag{20a}$$

$$A^+ = \frac{\beta}{2\Gamma(\omega^2 + R^2)}\{S_3\omega + S_4R - i(S_3R - S_4\omega)\}, \tag{20b}$$

and

$$A^- = \frac{\beta}{2\Gamma(\omega^2 + R^2)}\{S_3\omega - S_4R - i(S_3R + S_4\omega)\}, \tag{20c}$$

with

$$S_3 = [(\Delta + S_1)/2]^{1/2}, \quad S_4 = [(\Delta - S_1)/2]^{1/2}, \tag{20d}$$

and

$$\Delta = (S_1^2 + S_2^2)^{1/2}, \quad S_1 = 4\Gamma(\omega^2 - R^2)^2 + \Lambda^2, \quad S_2 = 8\Gamma R\omega. \tag{20e}$$

The pair of quadratic equations in Eq. (19) can give us four roots in general. Thus, the feedback processes create a situation where new modes may be introduced. Since our primary objective is to study the modification of the free traveling waves by the moist processes, we shall consider the nondissipative case first.

With $R = 0$, Eq. (19) reduces to a single quadratic equation in $k$ given by

$$k^2 + \left\{\frac{\beta}{\omega} + \frac{i\Lambda}{\Gamma}\right\}k - \frac{1}{\Gamma}\left[\omega^2 - \frac{\beta}{2\omega}(\Lambda^2 + 4\Gamma\omega^2)^{1/2} - \frac{i\beta\Lambda}{2\omega}\right] = 0. \tag{21}$$

It is clear from Eq. (21) that in the absence of the evaporation–wind feedback ($\Lambda = 0$), all the coefficients of the equation become real and the solutions may be written as

$$k = -\frac{\beta}{2\omega} \pm \frac{1}{2}(\beta/\omega - 2\omega/\Gamma^{1/2}). \tag{22}$$

Thus, it is clear that the wave–CISK by itself cannot make the mixed Rossby–gravity mode unstable. How-

ever, it can modulate the degree of instability set in by the evaporation–wind feedback mechanism. We also note that Eq. (21) allows two branches of solutions. In the dry case, one of the branches (westward-propagating Kelvin-like mode) is not allowed as it becomes unbounded. However, in the presence of the evaporation–wind feedback, both these branches are allowed. As we show clearly in section 4, the eigenfunctions corresponding to both these branches are bounded. Thus, evaporation–wind feedback introduces a new normal mode in the moist tropical atmosphere.

We note that solutions of Eq. (21) may have nontrivial imaginary components of wavenumber $k_i$. From Eq. (11), this represents a spatially growing or decaying component given by $\exp(-k_i x)$. However, spatial growth depends on the direction of phase propagation of the wave. For example, if a westward-propagating mode ($k_r < 0$) has $k_i > 0$, it would appear to decay in the positive $x$ direction in space. Since the wave is propagating in the negative $x$ direction, the wave in fact is growing in the direction of propagation. Therefore, we can represent the spatially growing part in terms of an equivalent temporally growing part given by $\exp(-\gamma t)$, where the growth rate $\gamma$ is given by $\gamma = -k_i k_r \omega/(k_r^2 + k_i^2)$. Thus, the modes with opposite signs of $k_i$ and $k_r$ are the ones that are temporally growing.

*a. General solution of the dispersion relation*

Since $\beta = \frac{1}{2}$, the general solution of Eq. (21) may be written as

$$k = -\frac{1}{2}\left(\frac{1}{2\omega} + \frac{i\Lambda}{\Gamma}\right) \pm \frac{1}{2}\left[\frac{1}{4\omega^2} + \frac{4\omega^2}{\Gamma} - \frac{\Lambda^2}{\Gamma^2} - \frac{1}{\omega\Gamma}(\Lambda^2 + 4\omega^2\Gamma)^{1/2}\right]^{1/2}. \quad (23)$$

Let us denote the quantity within the square bracket by $D$. We note that $D$ is always real, but could be positive or negative. When $D$ is positive, the solutions can be written as

$$k = \left\{-\frac{1}{4\omega} \pm D^{1/2}/2\right\} - \frac{i\Lambda}{2\Gamma}. \quad (24a)$$

On the other hand, when $D$ is negative, the solutions may be

$$k = -\frac{1}{4\omega} + i\left(-\frac{\Lambda}{2\Gamma} \pm \frac{1}{2}|D|^{1/2}\right). \quad (24b)$$

We note from Eq. (24a) that when $D$ is positive in the low-frequency domain, $D^{1/2}$ will be less than $1/(2\omega)$ and thus, both the modes will be westward propagating, one with $k_r$ large (short wavelength) and the other with $k_r$ small (long wavelength). Both of these waves will be damped and have the same damping rate. On the other hand, when $D$ is positive in the high-frequency regime, $D^{1/2}$ is larger than $1/(2\omega)$. Thus, in the high-frequency range, one solution is eastward propagating ($k_r > 0$) while the other is westward propagating ($k_r < 0$). We can also see that the eastward-propagating wave is unstable while the westward-propagating wave is damped. The growth rate of the unstable wave is equal to the damping rate of the stable wave. We also note that for reasonable values of $\Lambda$ and $\Gamma$, $D$ is always positive in the high-frequency regime.

For any reasonable combination of $\Lambda$ and $\Gamma$ (e.g., $\Lambda \sim 1$ and $\Gamma$ between 0.01 and 1), there always exists a range of $\omega$ in the low-frequency range for which $D$ is negative. The solutions, in this case, are given by Eq. (24b). Referring to the two solutions as branch 1 and branch 2, we note that, in this frequency range, the two branches correspond to two distinct westward-propagating waves with same $k_r$ but with different $k_i$. We also note that if $|D|^{1/2}$ is greater than $\Lambda/\Gamma$, one of the westward-propagating low-frequency waves would be unstable.

With these preliminary remarks, both the solutions of Eq. (23) are computed for a typical tropical atmosphere with $\Gamma = 0.5$ and $\Lambda = 0.5$. The real parts of these solutions are shown in the top panel of Fig. 1 by thin solid lines where the two solutions are denoted as

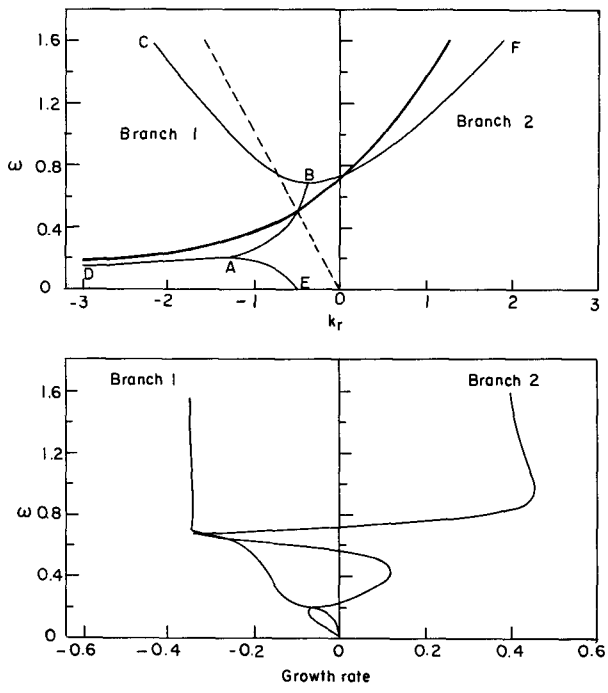


FIG. 1. Dispersion curves for the standard case ($\Gamma = 0.5$, $\Lambda = 0.5$, $R = 0$). Upper panel shows the variation of real wavenumber $k_r$ with frequency (thin solid line). The thick solid line represents the MRG mode for the dry atmosphere ($\Gamma = 1$, $\Lambda = 0$) and the thin dashed line represents the unbounded solution for the dry atmosphere. The growth rates, $\gamma$, for both the branches are shown in the lower panel. All variables are in nondimensional units.

branch 1 (DABC) and branch 2 (EABF). The thick solid line in this panel represents the MRG mode in the dry atmosphere with $\Gamma = 1$ and $\Lambda = 0$. The thin dashed line represents the solution of the dispersion relation in the dry atmosphere that is unbounded (hence not allowed). We note that both branches collapse to one between A and B. The corresponding growth rates ($\gamma$) for the two branches are shown in the lower panel of Fig. 1. We note that branch 1 is always damped. Branch 1 is the new solution allowed in the moist atmosphere. However, as it is always damped, it may not be observed. We shall show later that for a certain range of forcings, this branch could be nearly neutral. Branch 2 represents the modified MRG wave in the presence of moist processes. We note that the evaporation–wind feedback makes the MRG wave unstable in two frequency regimes. One unstable regime is in the low-frequency range, while the other is in the high-frequency range. It is of interest to note that the growth rate curve has a maximum in the low-frequency regime. This indicates a maximally growing mode that may be observed. For the set of parameters considered here ($\Gamma = 0.5$, $\Lambda = 0.5$, $R = 0$), the maximally growing low-frequency westward-propagating mode has $\omega = 0.45$, $k_r = -0.56$, and $k_i = 0.16$. This corresponds to a wave with period 3.3 days and a wavelength of about 12.3 thousand kilometers with $e$-folding time of about 1.8 days.

## 4. The eigenfunctions

Here we study the structure of the eigenfunctions for the $n = 0$ modes in the absence of dissipation ($R = 0$). Thus, $\sigma = \omega$. Combining Eqs. (14.3) and (17) and making use of Eq. (14.1), we may express the meridional velocity as

$$v(\Psi) = \exp\left[-\frac{1}{2}\left(1 - \frac{i}{2}\frac{\Lambda}{2\omega\Gamma C_1^{1/2}}\right)\Psi^2\right]. \quad (25.1)$$

From Eq. (12), making use of the transformation $\Psi = C_1^{1/4}y$, we can write $u(\Psi)$ and $\theta(\Psi)$ in terms of $v(\Psi)$ as

$$u(\Psi) = \frac{i}{\omega^2 - \hat{\Gamma}k}\left\{\frac{\omega y v}{2} - C_1^{1/4}\Gamma k\frac{dv}{d\Psi}\right\}, \quad (25.2)$$

and

$$\theta(\Psi) = \left[-\frac{i}{\omega^2 - \hat{\Gamma}k}\left\{\frac{\Gamma y v}{2} - C_1^{1/4}\Gamma\omega\frac{dv}{d\Psi}\right\}\right]. \quad (25.3)$$

In writing Eq. (25), we have made use of the fact that $H_0(\Psi) = 1$. The expressions in Eq. (25), together with Eq. (11), may be simplified to give the eigenfunctions as

$$v(x, y, t) = \cos\phi\exp(-k_i x - C_1^{1/2}y^2/2), \quad (26.1)$$

$$u(x, y, t) = -(U_1\cos\phi + U_2\sin\phi)y \times \exp(-k_i x - C_1^{1/2}y^2/2), \quad (26.2)$$

$$\theta(x, y, t) = (\Theta_1\cos\phi - \Theta_2\sin\phi)y \times \exp(-k_i x - C_1^{1/2}y^2/2), \quad (26.3)$$

where

$$\phi = k_r x - \omega t + \Lambda y^2/8\omega\Gamma, \quad (27.1)$$

$$U_1 = \Delta_I\omega/4 + \Gamma C_1^{1/2}(k_r\Delta_I - k_i\Delta_R) - \Lambda(\Delta_I k_i + \Delta_R k_r)/4\omega \quad (27.2)$$

$$U_2 = \Delta_R\omega/4 + \Gamma C_1^{1/2}(k_r\Delta_R - k_i\Delta_I) - \Lambda(\Delta_R k_i + \Delta_I k_r)/4\omega \quad (27.3)$$

$$\Theta_1 = \Delta_I\Gamma(k_r/4 + C_1^{1/2}\omega) + \Delta_R(\Gamma k_i/2 + \Lambda/2)/2, \quad (27.4)$$

$$\Theta_2 = \Delta_I(\Gamma k_i/2 + \Lambda/2)/2 - \Delta_R\Gamma(k_r/4 + C_1^{1/2}\omega), \quad (27.5)$$

with

$$\Delta_R = [\omega - \Gamma(k_r^2 - k_i^2) + \Lambda k_i] \times \{[\omega^2 - \Gamma(k_r^2 - k_i^2) + \Lambda k_i]^2 + (2\Gamma k_i + \Lambda)^2 k_r^2\}^{-1} \quad (27.6)$$

and

$$\Delta_I = [(2\Gamma k_i + \Lambda)k_r] \times \{[\omega^2 - \Gamma(k_r^2 - k_i^2) + \Lambda k_i]^2 + (2\Gamma k_i + \Lambda)^2 k_r^2\}^{-1}. \quad (27.7)$$

Several points may be noted from Eqs. (25) and (26).

(i) First, the meridional wind is symmetric about the equator, while the zonal wind and potential temperature perturbations associated with this mode are antisymmetric about the equator with maxima away from the equator.

(ii) We also note that due to the existence of the evaporation–wind feedback ($\Lambda > 0$), the singularity in the zonal wind and potential temperature eigenfunctions is removed. As mentioned in the previous section, this introduces the possibility of a new mode in the moist tropical atmosphere.

(iii) The term $\exp(-C_1^{1/2}y^2\ 2^{-1})$ represents the exponential decay of the eigenfunctions with latitude. Since $C_1 = (1 + \Lambda^2/4\omega^2\Gamma)/4\Gamma$ reduces to just ¼ in the dry atmosphere, the $e$-folding distance in the meridional direction for the dry atmosphere is $2L_0$. Both wave–CISK ($\Gamma$) and evaporation–wind feedback ($\Lambda$) increase $C_1$ and hence reduce the $e$-folding distance. Thus, the MRG waves are more strongly trapped around the equator in the moist atmosphere. Moreover, the evaporation–wind feedback makes the $e$-folding distance frequency dependent. The low-frequency

waves are more strongly trapped than the high-frequency waves in a moist atmosphere.

(iv) Another significant modification of the MRG wave eigenfunctions due to the moist processes is the introduction of wavy structure within the exponentially decaying envelope. Comparing Eqs. (26.1) and (27.1), it is easy to see that the meridional velocity will have nodes in the meridional direction when $\Lambda y^2/4\omega\Gamma = n\pi/2$ is satisfied. However, it is not so easy to see the nodes for the zonal wind and potential temperature perturbations. This indicates that the moist processes introduce a certain amount of complex meridional phase propagation in the $n = 0$ waves. However, this meridional phase propagation cannot be described in terms of a simple plane wave propagation.

Following these general comments, we examine in detail the basic structure of the eigenfunctions for the two branches. By basic structure we mean the structure of the eigenfunctions given by Eq. (26) without the $\exp(-k_i x)$ term, as this term represents only the spatially (or equivalently temporally) growing (or damped) part. We examine this at two frequency regimes, one in the low-frequency regime where one of the modes is maximally growing ($\omega \approx 0.45$ in Fig. 1), and another in the high-frequency regime (around $\omega \approx 1.0$). The two pairs of solutions selected in this manner from the standard case ($\Gamma = 0.5$, $\Lambda = 0.5$, $R = 0$) are

(i) $\omega = 0.45$, $k_r = -0.56$, $k_i = -1.17$ and $\gamma = -0.175$;

(ii) $\omega = 0.45$, $k_r = -0.56$, $k_i = 0.16$ and $\gamma = 0.12$;

(iii) $\omega = 1.033$, $k_r = 0.836$, $k_i = -0.50$ and $\gamma = 0.453$;

(iv) $\omega = 1.033$, $k_r = -1.324$, $k_i = -0.50$ and $\gamma = -0.34$.

The first one is a westward-propagating low-frequency damped wave, while the second one is a westward-propagating low-frequency growing wave. Similarly, the third one is an eastward-propagating high-frequency growing wave while the fourth one is a westward-propagating high-frequency damped wave.

The basic eigenfunctions for (i) the low-frequency westward-propagating damped wave are shown in Fig. 2. In the $x$ direction the eigenfunctions are plotted for one wavelength. The important point to note is that there exists a strong positive correlation or a nearly in-phase relationship between the zonal wind and potential temperature perturbations. This is consistent with the energy constraints for a damped wave, as discussed in section 2.

Figure 3 shows the basic eigenfunctions for the second wave (ii), i.e., the westward-propagating low-frequency unstable wave. The meridional scale of this

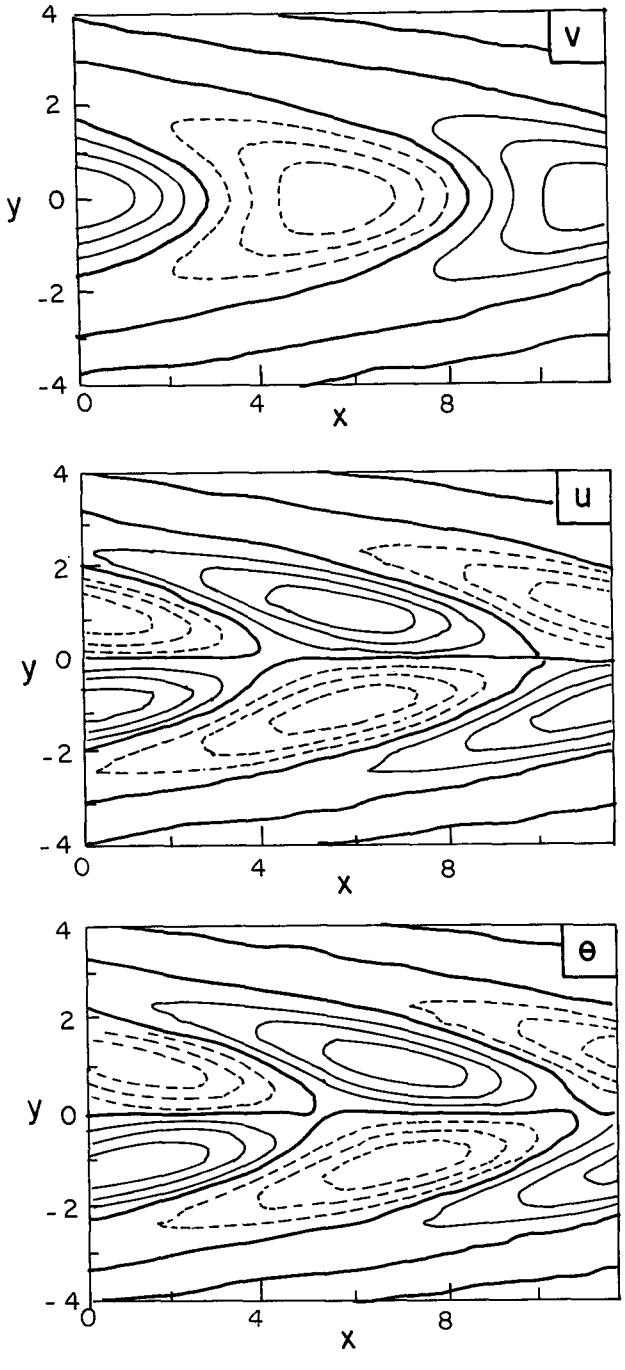


FIG. 2. Structure of the basic eigenfunctions [without the $\exp(-k_i x)$ term] for a damped low-frequency westward-propagating wave for the standard case with $\omega = 0.45$, $k_r = -0.56$, $k_i = -1.17$, and $\gamma = -0.175$. This is in the region (Fig. 1) where the two branches overlap. Each eigenfunction is normalized with respect to its maximum value and the contour interval is 0.25. Positive regions are solid and the negative regions are dashed lines. The thick solid line represents zero contour.

wave is very similar to that of the damped wave for the same frequency (Fig. 2). However, the significant difference between this and the damped wave is evident in the phase relationships between the zonal wind and potential temperature perturbations. For this unstable wave a negative correlation or a nearly out-of-phase relationship between $u$ and $\theta$ fields is clearly seen.

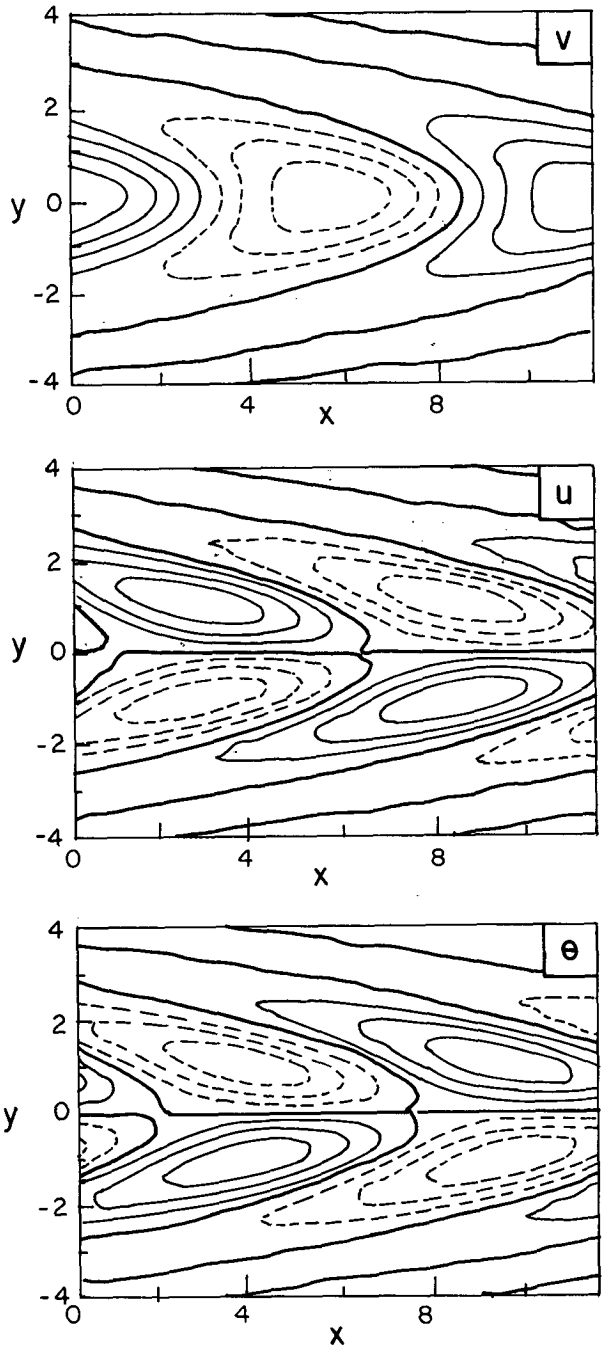


FIG. 3. Same as in Fig. 2 but for the growing mode with the same frequency and $k_r$. This mode has $\omega = 0.45$, $k_r = -0.56$, $k_i = 0.16$, and $\gamma = 0.12$.

Figures 4 and 5 show the basic eigenfunctions for (iii) the high-frequency eastward-propagating unstable wave and (iv) the high-frequency westward-propagating damped wave for the same frequency. Again, we note that the unstable wave (Fig. 4) has a negative correlation between $u$ and $\theta$, while the damped wave (Fig. 5) has a positive correlation between $u$ and $\theta$. Moreover, as discussed earlier in this section, the meridional scale of the high-frequency waves (Figs. 4 and 5) is much larger than the meridional scale of the low-frequency waves (Figs. 2 and 3). Also, the positive and negative phases within the decaying envelope in the meridional direction at a given longitude, introduced by the moist feedbacks, are clearly seen in these figures.

## 5. Sensitivity of the modes to changes in the strengths of feedbacks

In this section, we show how splitting of the MRG waves into two branches and the associated growth (or decay) rates depend on the strength of the feedback processes. As discussed in section 2, the wave–CISK (or convergence feedback) by itself cannot cause the splitting and growth of these waves. However, in the presence of evaporation–wind feedback ($\Lambda$), it can modulate the splitting as well as the growth rates. Here $\Gamma = 1$ represents the no-wave–CISK case while $\Gamma = 0$ represents the moist neutral case. Thus, we shall consider $0 < \Gamma \leq 1$. Similarly, we shall vary $\Lambda$ between 0 and 2; $\Lambda = 2$ represents a strong evaporation–wind feedback case. In Fig. 6 we show how the two branches of MRG waves evolve with four values of the strength of the evaporation wind feedback ($\Lambda = 0.15$, 0.6, 1.2, and 2.0) when there is no convergence feedback ($\Gamma = 1$) and no dissipation ($R = 0$). The top panel shows the real part of wavenumber $k_r$ and the lower panels show the corresponding growth rates, $\gamma = -k_r k_i \omega/(k_r^2 + k_i^2)$, as a function of frequency $\omega$. The first thing we note is that the growth rate of the low-frequency westward-propagating mode increases with the increase of the strength of the evaporation–wind feedback. The maximum growth rate for the low-frequency westward-propagating wave tends to occur at a slightly higher frequency (lower period) with the increase of evaporation–wind feedback. The high-frequency and low-frequency regimes of these results with $\Gamma = 1$, $R = 0$ are consistent with the discussions for these limits made in section 3a. It is of particular interest to note the nearly equal growth rates and damping rates for the two branches in the high-frequency limit. Another interesting point to note is that the range of frequencies over which the two branches collapse increases rapidly with the increase of the evaporation–wind feedback. As an example, for the weak strength of the evaporation–wind feedback considered here ($\Lambda = 0.15$), the

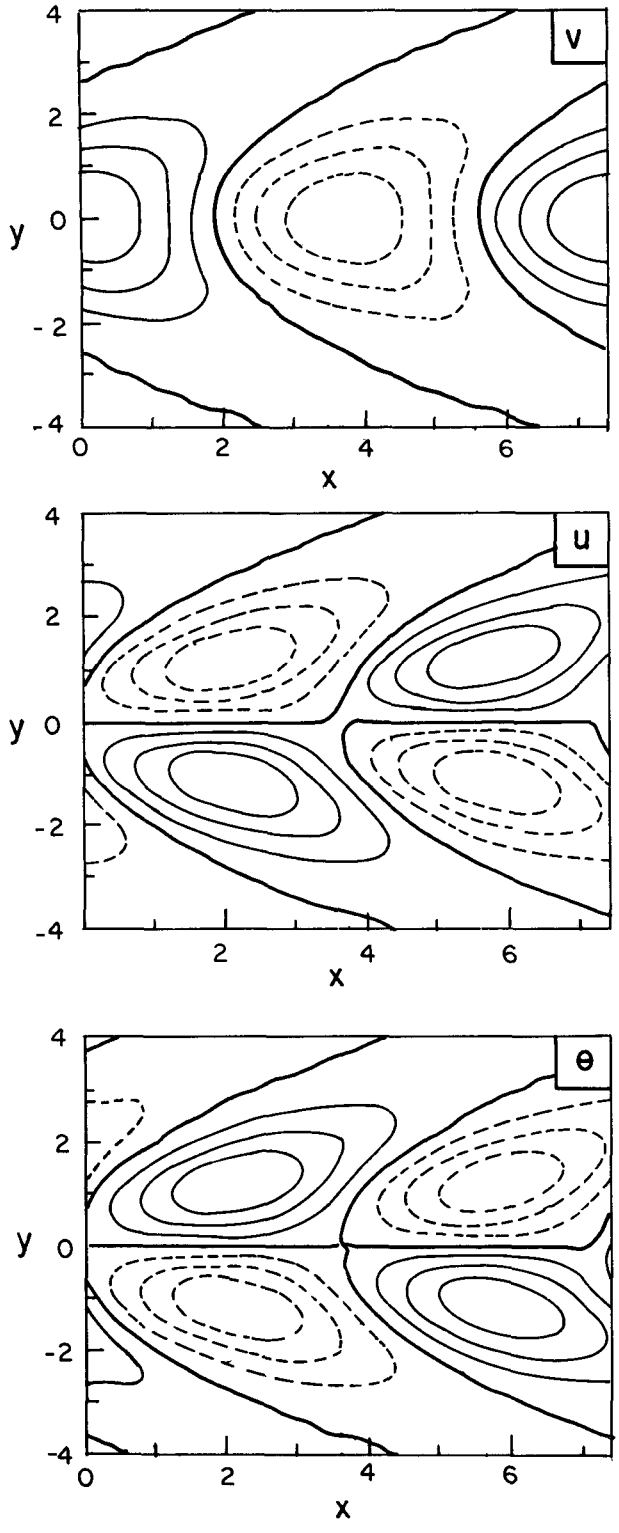


FIG. 4. Same as in Fig. 2, but for an eastward-propagating high-frequency growing mode with $\omega = 1.033$, $k_r = 0.836$, $k_i = -0.503$, and $\gamma = 0.453$.

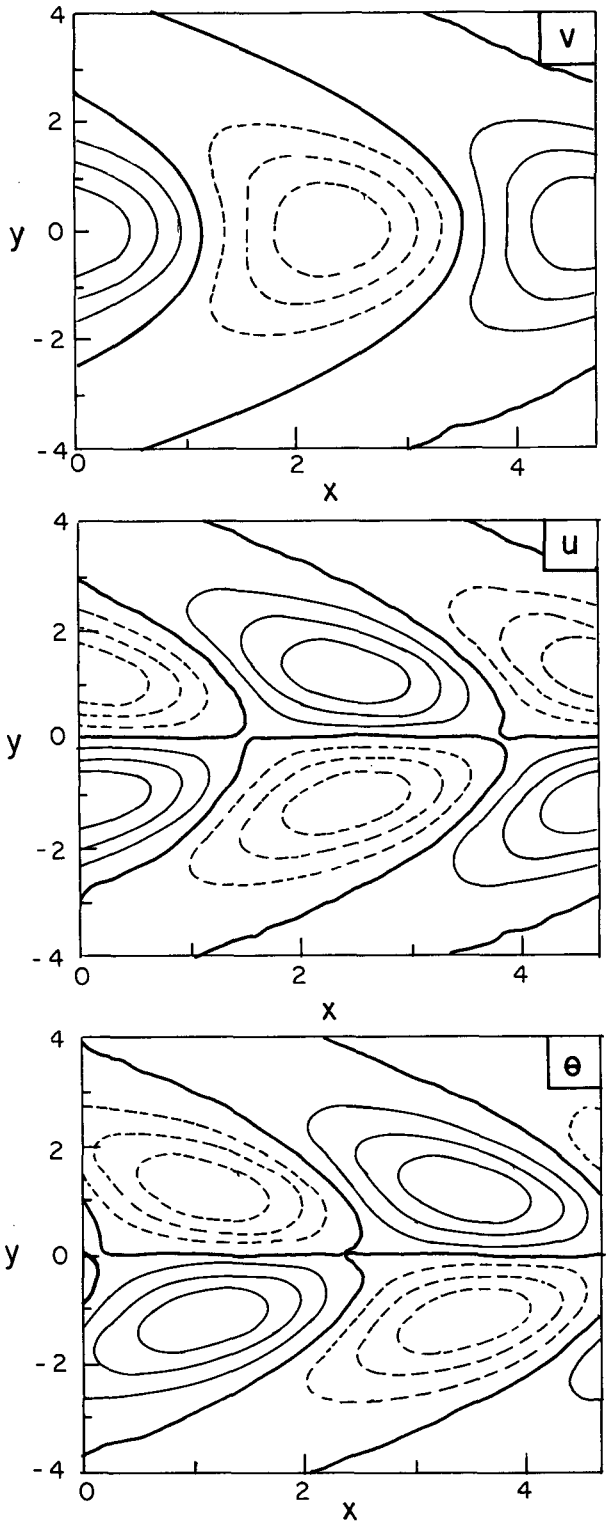


FIG. 5. Same as Fig. 2 but for an eastward-propagating high-frequency damped mode. For this mode, $\omega = 1.033$, $k_r = -1.324$, $k_i = -0.503$, and $\gamma = -0.34$.

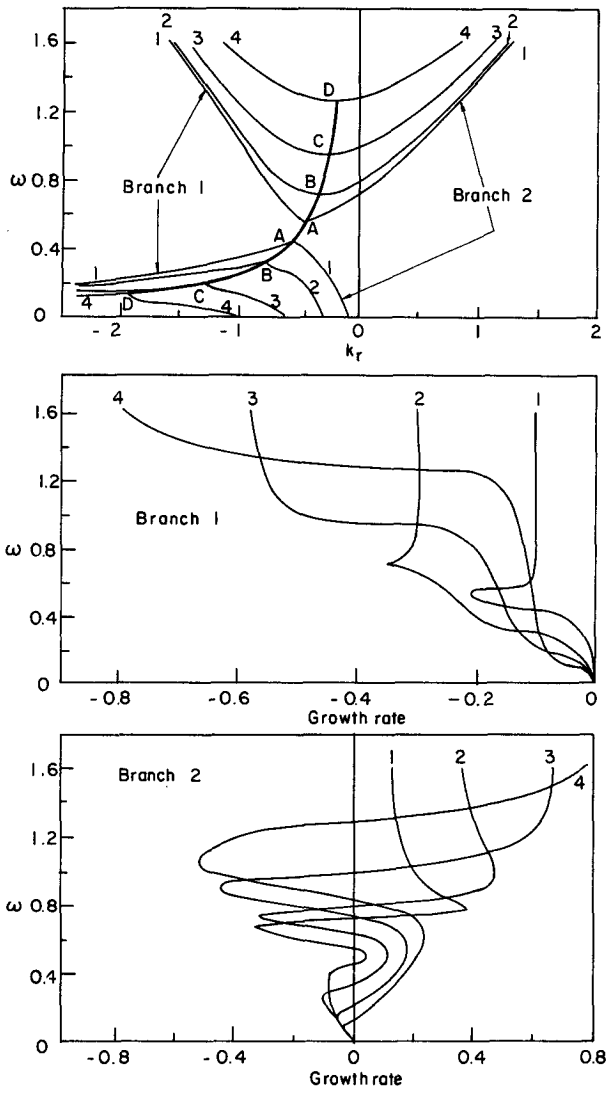


FIG. 6. Sensitivity of the dispersion relation to the strength of evaporation–wind feedback ($\Lambda$) in the absence of wave–CISK ($\Gamma$ = 1.0). The four sets of curves labeled 1 to 4 correspond to $\Lambda$ = 0.15, 0.6, 1.2, 2.0, respectively. The top panel represents a variation of real wavenumber $k_r$ as a function of $\omega$. The lower two panels show the growth rates ($\gamma$) for branch 1 and branch 2, respectively. As in Fig. 1, all the variables are in nondimensional units.

two branches overlapped over the region denoted by AA, while for the strong evaporation–wind feedback considered here ($\Lambda$ = 2.0), the range increases to DD. This is also associated with an increase in the unstable range for the low-frequency regime (lowest panel, Fig. 6).

In Figs. 7 and 8 we show the evolution of the new mode and the modified MRG wave with increased strength of the convergence feedback. Figure 7 is a repetition of Fig. 6 but with $\Gamma$ = 0.1, while Fig. 8 is a repetition of Fig. 6 but with $\Gamma$ = 0.01. Two important points may be made from these figures. First, the maximum growth rate for the low-frequency westward-propagating mode occurs at a lower frequency for higher strengths of convergence feedback. Second, for higher strength of the convergence feedback the first branch becomes nearly neutral for nearly all frequencies even with moderate strength of the evaporation–wind feedback (e.g., $\Gamma$ = 0.01, $\Lambda$ = 0.6). Moreover, we note that the range of frequencies over which the two branches overlap for a given strength of evaporation–wind feedback increases considerably with the increase of the strength of the wave–CISK. For example, the range denoted by BB over which the two branches overlap for moderate strength of evaporation–wind feedback ($\Lambda$ = 0.6) corresponds to a frequency range

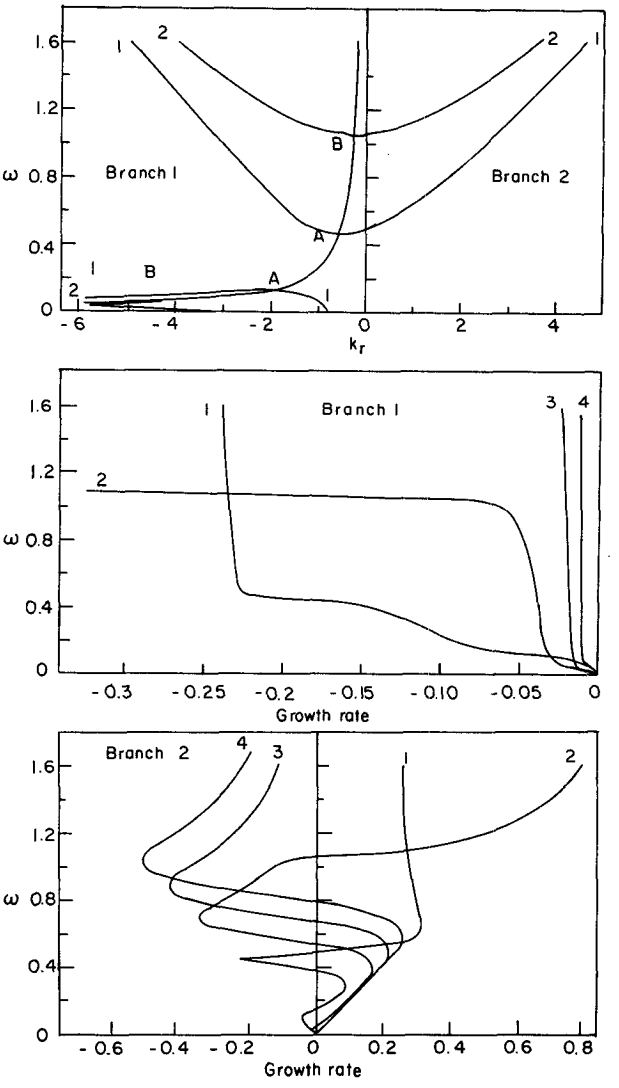


FIG. 7. Same as in Fig. 6 but for a moderate strength of wave–CISK ($\Gamma$ = 0.1). All other conventions are same as in Fig. 6. Here, the curves 3 and 4 are out of range in the top panel.

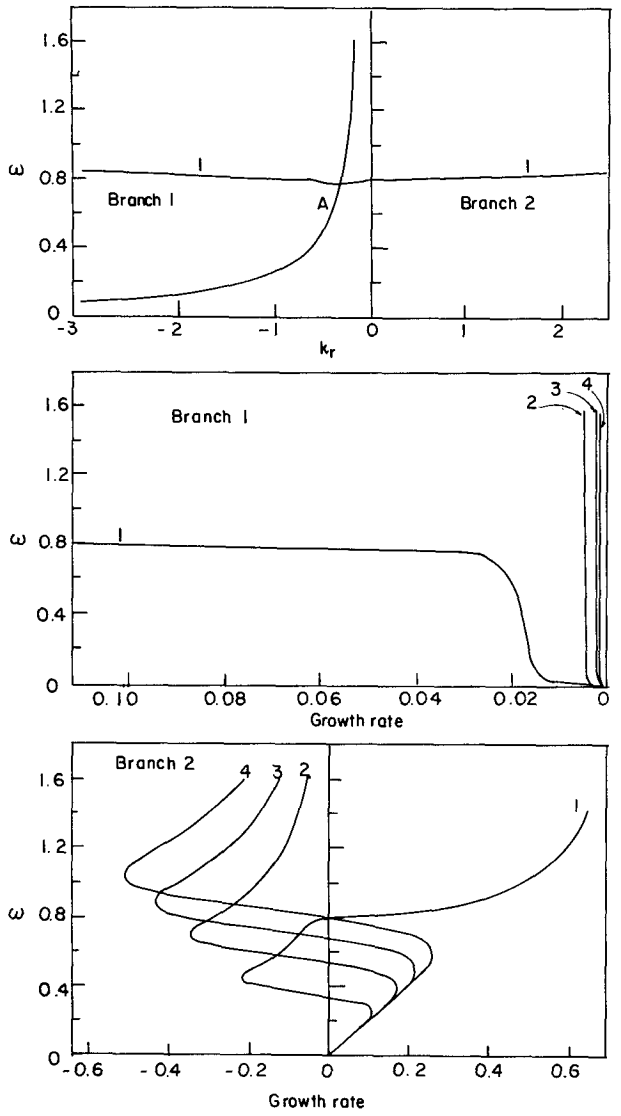


FIG. 8. Same as in Fig. 6 but in the presence of a strong wave–CISK feedback ($\Gamma = 0.01$). All other conventions are same as in Fig. 6. Here, the curves 2, 3, and 4 are out of range in the top panel.

$\delta_\omega$ of about 0.45 with $\Gamma = 1.0$ (Fig. 6). For $\Gamma = 0.1$ it increases to about 1.0 and for $\Gamma = 0.01$, it goes beyond the range of frequencies shown in Fig. 8. Comparing Figs. 6–8, we also note that for the same strength of evaporation–wind feedback, an increase in wave–CISK increases the unstable range for the low-frequency westward-propagating unstable mode.

So far we have confined our discussion to the non-dissipative case. To understand how the presence of a small amount of dissipation would modify these waves, we solved the general dispersion relation [Eq. (19)] for specified strengths of convergence feedback and evaporation–wind feedback ($\Gamma = 0.01$ and $\Lambda = 0.5$) for three values of dissipation ($R = 0.01, 0.05, 0.08$). These represent dissipation time scales of 22, 4.5, and 2.75 days, respectively. These results are shown in Fig. 9. The most interesting point is that the splitting between the two branches becomes clear in the presence of dissipation. The region over which the two branches overlapped in the absence of dissipation becomes separated (top panel of Fig. 9). The gap between the two branches increases with increasing dissipation. Moreover, the second branch becomes eastward propagating at very low frequencies as well as at high frequencies. It is also of interest to note that the dissipation increases

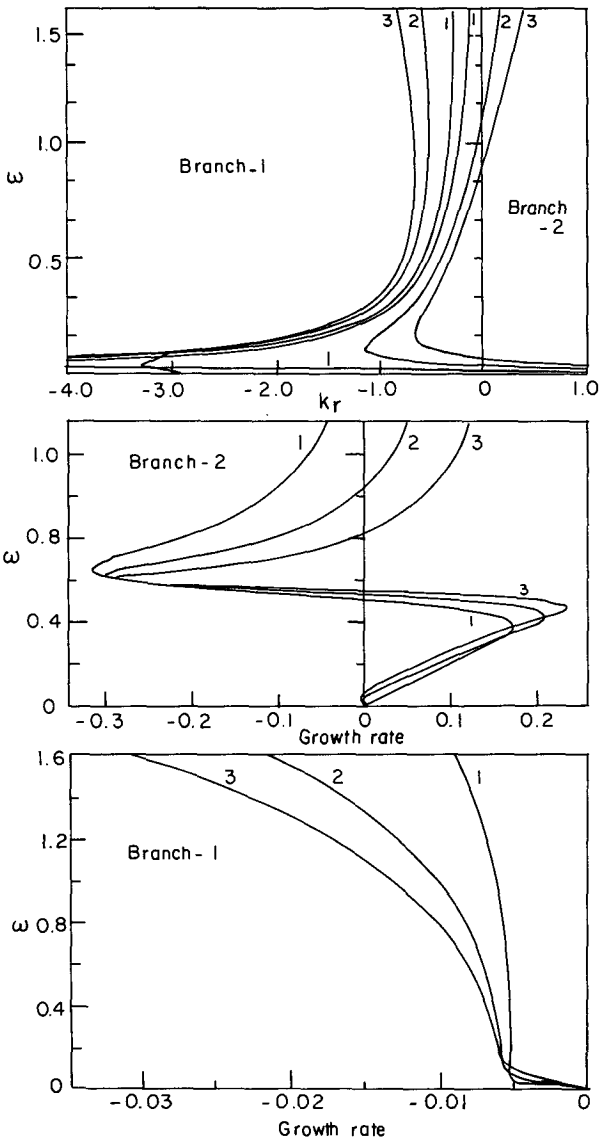


FIG. 9. Role of dissipation in the dispersion relation for the $n = 0$ waves. The curves 1, 2, and 3 in this figure correspond to $R = 0.01$, 0.05, and 0.08, respectively; the strengths of the feedbacks for this case are $\Gamma = 0.01$ and $\Lambda = 0.5$. Other conventions are similar to those of Fig. 6.

the growth rate of the low-frequency westward-propagating unstable mode.

The characteristics of the maximally growing low-frequency westward-propagating mode are summarized in Table 1 for different strengths of the feedbacks.

## 6. Discussions and conclusions

The modification of the $n = 0$ modes by evaporation–wind feedback and wave–CISK is studied in detail. The moist processes introduce a new westward-propagating mode, in addition to dramatically modifying the dry MRG mode. The new westward-propagating mode is damped but could be nearly neutral for strong wave–CISK feedback and moderate strength of evaporation–wind feedback. The major new result is that the evaporation–wind feedback modifies the dry MRG wave and drives it unstable over two frequency regimes. One unstable region is in the low-frequency domain while another unstable region is in the high-frequency domain. The low-frequency unstable MRG waves are westward propagating and are of considerable practical interest. The range of unstable frequencies and the growth rate, as well as the frequency at which maximum growth rate occurs for the low-frequency westward-propagating unstable mode, increase with the increase in the evaporation–wind feedback for a given strength of wave–CISK. As the strength of the wave–CISK increases, the maximum growth rate for the low-frequency westward-propagating unstable MRG mode occurs at a lower frequency for a given strength of the evaporation–wind feedback.

The moist processes also introduce two significant modifications in the eigenfunctions of the MRG mode. The meridional decay scale for the dry MRG waves is given by $\exp(-y^2/4)$ and is the same for the low-frequency as well as the high-frequency waves. In the presence of evaporation–wind feedback, this decay scale becomes frequency dependent and varies inversely with frequency. Thus, the low-frequency waves are more tightly trapped around the equator than the high-frequency waves in a moist atmosphere. The other qualitative modification the evaporation–wind feedback introduces is a rather complex meridional phase propagation of the mode. This manifests in the eigenfunction as positive and negative phases in the meridional direction within the decaying envelope at a given longitude. This further reduces the effective meridional scale of these waves.

From Table 1 we note that for reasonable strengths of wave–CISK and evaporation–wind feedback the maximally growing low-frequency westward-propagating mode has period of about 4.5 days and wavelength of about 8000 km (e.g., for $\Lambda = 0.25$, $\Gamma = 0.1$). (The corresponding phase speed of the wave is about 12 m s$^{-1}$.) Depending on the strengths of the feedbacks, the period can vary from 3 to 7 days while the wavelength can vary from 14 000 km to 5600 km. The corresponding variation of the westward phase speed is between 5.5 m s$^{-1}$ and 29 m s$^{-1}$.

Takayabu and Murakami (1991) find that there are two westward-propagating waves with period around 4 days, in the cloudiness as well as in the lower tropospheric winds in the western Pacific. One wave has faster phase speed of about 14–19 deg day$^{-1}$ with wavelength of about 6000 km, while the other has slower phase speed of about 6–10 deg day$^{-1}$ and wavelength of about 2500 km. The long-wave, faster, westward-propagating mode has meridional velocity maximum around the equator and zonal wind maximum and cloudiness maximum about 7.5 deg away from the equator (Takayabu and Murakami 1991, Fig. 4). Similarly, Liebmann and Hendon (1990) identify a westward-propagating mode with period of about 4 days using eight years of analyzed meridional winds and other fields in the lower troposphere. They also find that this westward-propagating mode in the western Pacific has a wavelength of about 6700 km and a phase speed of about 18 m s$^{-1}$ (approx. 15 deg day$^{-1}$). Their analysis of other fields indicates that this is also an equatorially trapped MRG-type wave. Thus, this mode

TABLE 1. Characteristics of the maximally growing westward-propagation low-frequency mode for different strengths of the feedbacks.

| | $\Gamma = 0.1$ | | | | $\Gamma = 0.01$ | | | |
|---|---|---|---|---|---|---|---|---|
| $\Lambda$ | Period (days) | Wavelength ($10^3$ km) | Phase speed (m s$^{-1}$) | $E$-folding time (days) | Period (days) | Wavelength ($10^3$ km) | Phase speed (m s$^{-1}$) | $E$-folding time (days) |
| 0.05 | 4.8 | 8.3 | −11.4 | 7.1 | 7.2 | 5.6 | −29.1 | 3.4 |
| 0.15 | 4.8 | 8.3 | −12.3 | 2.8 | 5.4 | 7.4 | −18.1 | 2.1 |
| 0.25 | 4.3 | 9.3 | −10.6 | 2.0 | 4.8 | 8.3 | −15.2 | 1.7 |
| 0.35 | 3.9 | 10.0 | −9.0 | 1.7 | 4.3 | 9.3 | −12.5 | 1.5 |
| 0.45 | 3.6 | 11.0 | −7.7 | 1.5 | 3.9 | 10.0 | −10.3 | 1.4 |
| 0.55 | 3.6 | 11.0 | −8.1 | 1.4 | 3.6 | 11.0 | −8.5 | 1.3 |
| 0.65 | 3.3 | 12.0 | −6.9 | 1.3 | 3.3 | 12.0 | −7.1 | 1.3 |
| 0.75 | 3.3 | 12.0 | −7.2 | 1.2 | 3.3 | 12.0 | −7.4 | 1.2 |
| 0.85 | 3.1 | 13.0 | −6.0 | 1.2 | 3.1 | 13.0 | −6.2 | 1.1 |
| 0.95 | 3.1 | 13.0 | −6.3 | 1.1 | 3.1 | 13.0 | −6.4 | 1.1 |

is consistent with the long-wave, fast propagating mode found by Takayabu and Murakami (1991). Liebmann and Hendon (1990) also find a similar westward-propagating wave with period of about 4 days in the Atlantic, but it has somewhat shorter wavelength (~4500 km) and slower phase speed (~14 m $s^{-1}$). To our knowledge, no theory has so far explained the period and scale selection for these westward-propagating waves. Results of our study provide an explanation for the longer wavelength, westward-propagating wave observed in the central and the western Pacific. As discussed in the previous paragraph, the evaporation–wind feedback-driven, maximally growing, westward-propagating MRG wave has period of about 4.5 days, wavelength of about 8000 km, and phase speed of about 12 m $s^{-1}$ for modest strengths of the feedbacks. Considering the simplicity of our model, the agreement of the period and the wavelength with observations is remarkable. However, the phase speed given by our model is somewhat low. This is probably understandable as we have assumed a resting basic state. If we consider a mean easterly of about $-10$ m $s^{-1}$ and assume a simple Doppler shifting of the phase speed, we get a phase speed of about 22 m $s^{-1}$ which compares very well with the observed phase speed. We also note that there is a considerable amount of variability of the period, wavelength, and phase speed of the maximally growing westward-propagating mode with the variation of strength of the feedbacks. Another interesting feature emerges from our study of the sensitivity of the properties of the $n = 0$ modes to the various forcing parameters. While the appearance of a maximally growing westward mode is a relatively stable feature in the sense that it does not critically depend on the range of values of parameters, the various characteristics of the mode, in particular its period and wavelength, vary with the strengths of the feedbacks. Since the strengths of these feedbacks depend on the background conditions (such as sea surface temperature) which vary from region to region, our theory offers a natural explanation also for the observed quasi-periodicity of these tropical westward-propagating oscillations.

Holton (1972) showed that a heat source antisymmetric about the equator with maximum heating around 6–7 deg away from the equator with a period of about 4–5 days can force the observed MRG wave in the equatorial lower stratosphere with a period of about 5 days and wavelength of about 10 000 km. However, the source for the antisymmetric heat source with periodicity of about 4–5 days was not clear. Since the convergence for the low-frequency (4–5 days) unstable MRG mode discussed here occurs around 7 deg away from the equator, it offers a natural explanation for an antisymmetric heat source with desired period for forcing the observed MRG wave in the equatorial stratosphere.

In the formulation of evaporation–wind feedback it is assumed that the background mean winds are easterlies ($\Lambda > 0$). While this is true over the equatorial Pacific and Atlantic, it is not true over the Indian Ocean during Northern Hemispheric summer. In a future study, we show that the evaporation–wind feedback in the presence of mean westerlies modifies the $n = 0$ modes in such a way that it may explain the observed quasi-biweekly oscillations over this region (Krishnamurti and Bhalme 1976; Murakami 1976; Krishnamurti and Ardunay 1980).

One weakness in our study lies in the simplistic parameterization of the convergence feedback process. We have assumed that positive perturbation heating occurs in the regions of wave convergence, while negative perturbation heating occurs in the regions of wave divergence. Thus, the essential character of the positive-only heating associated with the wave convergence needs to be taken into account. However, it cannot be done in a simple analytical model. Another weakness may lie in the assumption of a single-mode vertical structure. How the horizontal structure of the different vertical modes would be modified by these feedbacks should be examined. Also, a prognostic equation for humidity with temperature dependence of $q_s$ taken into account must be included to discuss the above findings in a more general situation.

*Acknowledgments.* We thank Professor M. Sankar Rao for many discussions. The authors are grateful to two anonymous reviewers and Dr. I. M. Held for some insightful comments on an earlier version of this paper. Part of this work was sponsored by the Department of Science and Technology through Grant DST/BNG/CAS/131. Prashant Goswami would like to thank the Council for Scientific and Industrial Research for a fellowship. The authors thank Ms. K. Nagarathna for her help in preparing the manuscript.

## REFERENCES

Davey, M. K., 1985: Results from a moist equatorial atmosphere model. *Coupled Ocean Atmosphere Models.* J. C. J. Nihoul, Ed., Elsevier, Oceanographic Series, 41–49.

——, 1989: A simple tropical moist model applied to the 40-day wave. *Quart. J. Roy. Meteor. Soc.*, **115**, 1071–1107.

——, and A. E. Gill, 1987: Experiments on tropical circulation with a simple moist model. *Quart. J. Roy. Meteor. Soc.*, **113**, 1237–1269.

——, and G. Budin, 1989: Modelling intraseasonal and interannual variability in the tropics. *Phil. Trans. R. Soc. London*, **A329**, 155–166.

Emanuel, K. A., 1987: An air–sea interaction model of intraseasonal oscillations in the tropics. *J. Atmos. Sci.*, **44**, 2324–2340.

Gill, A. E., 1982: Spontaneously growing hurricane-like disturbances in a simple baroclinic model with latent heat release *Intense Atmospheric Vortices.* L. Bentsson, and J. Lighthill, Eds., Springer-Verlag, 111–130.

Hendon, H. H., 1988: A simple model of 40–50 day oscillation. *J. Atmos. Sci.*, **45**, 569–584.

Holton, J. R., 1972: Waves in the equatorial stratosphere generated by tropospheric heat source. *J. Atmos. Sci.*, **29**, 368–375.

Krishnamurti, T. N., P. K. Jayakumar, J. Sheng, N. Surgi and A. Kumar, 1985: Divergent circulation on the 30 to 50 day time scale. *J. Atmos. Sci.*, **42**, 364–375.

Knutson, T. R., and K. M. Weickmann, 1987: 30–60 day atmospheric oscillations: Composite life cycles of convection and circulation anomalies. *Mon. Wea. Rev.*, **115**, 1407–1436.

Lau, K. M., and P. H. Chan, 1986: Aspects of the 40–50 day oscillations during northern summer as inferred from outgoing longwave radiation. *Mon. Wea. Rev.*, **114**, 1354–1367.

——, and L. Peng, 1987: Origin of low frequency intraseasonal oscillations in the tropical atmosphere. Part I: Basic theory. *J. Atmos. Sci.*, **44**, 950–972.

——, and S. Shen, 1988: On the dynamics of intraseasonal oscillations and ENSO. *J. Atmos. Sci.*, **45**, 1781–1797.

Liebmann, B., and H. H. Hendon, 1990: Synoptic scale disturbances near the equator. *J. Atmos. Sci.*, **47**, 1463–1479.

Madden, R. A., 1986: Seasonal variations of the 40–50 day oscillation in the tropics. *J. Atmos. Sci.*, **43**, 3138–3158.

——, and P. R. Julian, 1971: Detection of a 40–50 day oscillation in the zonal wind in the tropical Pacific. *J. Atmos. Sci.*, **28**, 702–708.

——, and ——, 1972: Description of global scale circulation cells in the tropics with a 40–50 day period. *J. Atmos. Sci.*, **29**, 1109–1123.

Miyahara, S., 1987: A simple model of the tropical intraseasonal oscillation. *J. Meteor. Soc. Japan*, **65**, 341–351.

Murakami, T., and T. Nakazawa, 1985: Tropical 45-day oscillations during 1979 Northern Hemisphere summer. *J. Atmos. Sci.*, **42**, 1107–1122.

Neelin, J. D., I. M. Held and K. H. Cook, 1987: Evaporation wind feedback and low frequency variability in the tropical atmosphere. *J. Atmos. Sci.*, **44**, 2341–2348.

Parker, D. E., 1973: Equatorial Kelvin waves at 100 millibars. *Quart. J. Roy. Meteor. Soc.*, **99**, 116–129.

Pedlosky, J., 1979: *Geophysical Fluid Dynamics*. Springer Verlag. 624 pp.

Takahashi, M., 1987: A theory of the slow phase speed of the intraseasonal oscillation using the wave–CISK. *J. Meteor. Soc. Japan*, **65**, 43–49.

Takayabu, Y. N., and M. Murakami, 1991: The structure of super cloud clusters observed in 1–20 June 1986 and their relationship to easterly waves. *J. Meteor. Soc. Japan*, **69**(1), 105–125.

Weickmann, K. M., G. R. Lussky and J. E. Kutzbach, 1985: Intraseasonal (30–60 day) fluctuations in outgoing longwave radiation and 250 mb streamfunction during northern winter. *Mon. Wea. Rev.*, **113**, 941–961.

Yamagata, T., 1987: A simple moist model relevant to the origin of intraseasonal disturbances in the tropics. *J. Meteor. Soc. Japan*, **65**, 153–165.